Iranian Polymer Journal (2022) 31:1197–1208
https://doi.org/10.1007/s13726-022-01069-1

ORIGINAL RESEARCH

Chitosan-based electrolytes containing carbon nanotube-titanium dioxide for energy conversion devices applications

Naima Naffati[1,2,3] · Mariana Fernandes[4] · Verónica de Zea Bermudez[4] · Mohamed Faouzi Nsib[2,5] · Youssef Arfaoui[6] · Ammar Houas[2] · Joaquim Luis Faria[3,7] · Cláudia Gomes Silva[3,7] · Maria Manuela Silva[1]

Received: 25 October 2021 / Accepted: 16 April 2022 / Published online: 21 June 2022

Abstract

Polymer membranes based on natural polymer chitosan (CH) and variable content of carbon nanotube-titanium dioxide (CNT-TiO_2) composites were prepared by solvent casting at room temperature. The interest in natural polymers is enormous due to the depletion of oil and natural gas resources. Furthermore, the use of biodegradable biopolymers reduces the environmental impact of the disposal and avoids the long-term degradation of synthetic polymers. The thermal, morphological and electrochemical properties of the membranes were investigated by differential scanning calorimetry (DSC), thermogravimetric analysis (TGA), polarized optical microscopy (POM) and complex impedance spectroscopy. The obtained results revealed a predominantly semi-crystalline morphology and a satisfactory ionic conductivity. The sample with the highest conductivity was CH-20CNT-$TiO_{2\text{-}0.05}$, which attained 1.22×10^{-4} S cm^{-1} at 90 ºC. The significant effect of glycerol as a plasticizer on the conductivity of the materials was studied. The combination of Pt-based catalysts with TiO_2 led to a conductivity increase (90×10^{-3} S cm^{-1} at 90 °C). The conductivity measurements in the obtained composites allowed some evidence to be considered for the influence of CNT-TiO_2 in the transfer of current through the CH matrix. The encouraging properties (conductivity, thermal behaviour, morphology) of the samples lead us to suggest the incorporation of these materials as electrolytes in solid electrochemical devices. Composite membranes that are environmentally friendly and have attractive properties are developed for energy conversion device applications.

Graphical abstract

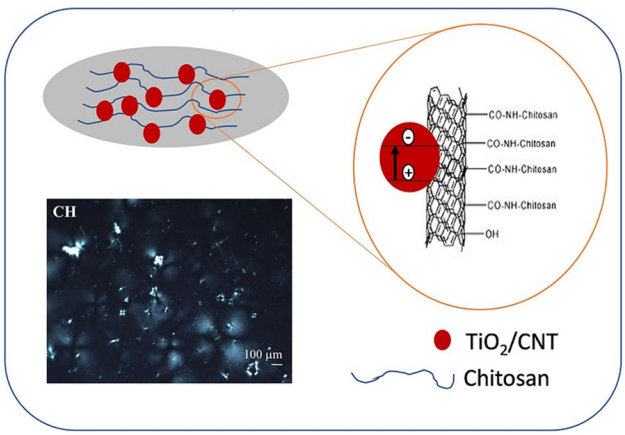

Keywords Carbon nanotubes · Titanium dioxide · Polymer electrolytes · Chitosan · Ionic conductivity

✉ Maria Manuela Silva
nini@quimica.uminho.pt

Extended author information available on the last page of the article

Introduction

The most attractive way to store energy to provide electrical power is to convert chemical into electrical energy [1]. The electrolyte is an ionic conductor that ensures ion transfer between the cathode and the anode. Electrolytes can take several different forms and phases (e.g., liquid, solid, gel, etc.). In general, liquid electrolytes have low viscosity and high ionic conductivity. However, they have leakage problems. The electrochemistry of non-aqueous solvents became essential between the 1950s and 1960s with the concept of lithium batteries [2]. Several salt-solvent combinations were explored over the years, and the maximum conductivity values were determined.

In this context, solid polymer electrolytes (SPEs) have been the focus of much attention as potential electrolytes of great technological relevance for solid-state electrochemistry, in particular, because of their practical application in devices, such as batteries, super capacitors, fuel cells, smart windows, sensors, and solar cells. Several advantages are associated with SPEs and compared with liquid electrolytes, SPEs have higher safety and thermal stability since they can provide a physical barrier layer to separate positive and negative electrodes and prevent thermal runaway under high temperature or impact. In addition, solid electrolyte makes it possible to use a lithium metal anode, due to the effective suppression of Li dendrite formation to promote long life time, low charge time and low internal corrosion. SPEs not only have excellent electrochemical performance and high safety but are also good in flexibility and processability, which have high possibilities for use in next-generation of devices. In addition, SPE can be fabricated extremely thin, which would limit the problems associated with poor ionic conductivity [3] and contribute to a much higher energy density [4]. However, SPEs also present some limitations: (1) lack of sufficient ionic conductivity to work properly at room temperature; (2) the interfaces between the SPE and cathode/anode, the stability during the charging process, the usage ratio of active material, and the interfacial resistance/compatibility can influence the available capacity and cycling stability of devices; and (3) facing the problem of maintaining the structural integrity of the SPE when subjected to stresses in the electrochemical cycling (cracks in the structure). SPEs for lithium-ion batteries applications should exhibit ionic conductivity values above 10^{-4} S cm^{-1} at room temperature [5, 6]. However, for fuel cells, SPEs can exhibit the same value, but at high temperatures [7].

SPEs constitute a class of materials whose physical and electrochemical properties are different from those of liquid electrolytes and conventional solids [8]. Since the pioneering studies of Wright et al. [9] and Armand et al. [10], polymer-based materials have been widely studied and continue to attract significant attention from researchers. Many systems involving several types of polymers, such as poly (propylene oxide) (PPO), poly (ethyleneimine) (PEI), and many doping salts, such as monovalent (Li^+, Na^+, Ag^+, etc.), divalent (Cd^{2+}, Ca^{2+}, Zn^{2+}etc.) and transition metals salts have been investigated. The structure of the polymers plays an important role in the properties of SPEs because they influence the conduction mechanism [11]. Natural polymers can be used as polymer host matrices in electrolytes. They present many advantages, such as low cost, non-toxicity, abundance in nature, and are environmentally friendly [12]. Several natural polymers have been used to prepare SPEs, such as starch [13], pectin [14], gelatine [15], cellulose [16], and chitosan (CH) [17–19], and etc.. CH can be prepared by deacetylation of chitin, one of the most abundant natural polysaccharides. The solubility of CH in common solvents largely exceeds that of chitin [20] due to the presence of NH_2 and OH functional groups which can act as electron donors and interact with inorganic salts [21, 22]. A CH film shows low conductivity and a way to improve it is to add a plasticizer, like glycerol [23]. Glycerol has been used as a plasticizer because of its compatibility with CH, which stimulates better mechanical properties. The plasticizer reduces the glass transition temperature and increases segmental motion, which results in an increase in conductivity [24–26]. The transport of the ions depends on several factors, such as the concentration of dopant, the dielectric constant of the polymer, and the mobility of ions within the polymer chains [27]. Despite the advances in the development of SPEs, there is still a large space for improvement. They are formed upon dispersion of different (nano) fillers (inert oxide ceramic, molecular sieves, metallic, etc.) in the polymer matrix with the goal of improving the mechanical, thermal and/or electrochemical properties [28]. In this way, the incorporation of suitable ionic liquids [29], nanoparticles (NPs) [30, 31], and fillers such as carbon nanotubes (CNTs) [32] into the polymer matrice has shown to be an interesting approach.

The most relevant properties of CNT are their high surface area, high electrical conductivity, and excellent thermal and mechanical properties [33, 34]. CNT/polymer membrane composites have been proposed for different purposes, such as filtration [35], sensing and monitoring systems [36]. In the particular case of batteries, CNTs have been mainly used for electrodes fabrication [37–39] and recently for battery separators. In the latter case, the CNT content must be below the electrical percolation limit, due to the need to obtain electronically insulator membranes with suitable ionic conductivity [40]. The successful use of fillers reported in our previous works [41, 42] reinforces the relevance of the present study aimed at investigating the effect of the CNT content and type on the polymeric matrix type, to prepare

membranes based on CH with enhanced properties. Further, SPE filled with CNT can also improve compatibility with the battery electrodes due to the carbonaceous nature of some of them [43, 44]. Other authors reported the use of CH and CNT to make membranes for energy conversion devices [45–48].

In this work, we study the combined use of CNTs and titanium dioxide (TiO_2), as dopants, to improve the conducting properties of the membranes. CNTs have a moderate stable morphology makes it possible to create proton transfer pathways. Moreover, nanocomposites of TiO_2 with CNTs (TiO_2-CNTs) are one of the most advanced nanomaterials that exhibit high performance and great flexibility [45, 49, 50].

We report the preparation and characterization of SPEs based on CH as host polymer, glycerol as plasticizer, and CNT-TiO_2 as filler. Moreover, we report the combination of Pt-based catalysts with TiO_2 as the catalyst support to evaluate the potential advantages of these combined materials for applications in fuel cells. In fuel cells, the SPE acts as a medium for proton exchange between electrodes. Fuel cells are promising technological alternatives to reduce our dependence on fossil fuels and emission of pollutants. Fuel cells are generally used for portable applications and transportation because they hold several advantages over conventional technologies, such as their high electrical efficiency, silence, no vibrations, and low or null pollutant emissions.

The thermal properties were evaluated by DSC and TGA, the morphological characteristics by POM, and the electrochemical features were measured by complex impedance spectroscopy and cyclic voltammetry. The wettability of the samples was assessed by means of static contact angle measurements.

Experimental

Nanoparticles (NPs) preparation

CNT-TiO_2 composites were prepared according to the procedure reported elsewhere [13]. For the synthesis of the CNT-TiO_2 composites, both CNT (Shenzhen Nanotech Port Co., Ltd. 0.2, 0.1 and 0.01 g, respectively) and TiO_2 (1.0 g Sigma-Aldrich 99.8% metal basis) were added simultaneously (one-pot) with 150 mL of nitric acid (HNO_3, Sigma-Aldrich 65% by wt) solution (functionalization of the CNTs with HNO_3 solution). The suspension was heated to 140 ºC and kept under magnetic stirring for 3 h in a round bottom flask equipped with a condenser. After cooling, the suspension was washed several times with distilled water, until the rinsing water was neutralized. The recovered powders were dried overnight at 110 °C. The resulting composite materials (the NPs) were labelled as xCNT-TiO_2, where x corresponds to the weight percentage of CNTs in the CNT-TiO_2composites (x = 1, 10 and 20%). The metal phase was loaded by incipient wetness impregnation from the aqueous solution of the platinum (Pt) salt (dihydrogen hexachloroplatinate (IV) hexahydrate, $H_2PtCl_6{\cdot}6H_2O$). The Pt content was fixed at 1% (by weight). After impregnation, the samples were dried at 100 °C for 24 h. The catalysts were then heat treated under nitrogen flow for 1 h and reduced under hydrogen for 3 h at 200 °C. The temperatures were selected based on a preliminary "temperature programmed reduction" (TPR) analysis of given metal-loaded TiO_2 materials, which revealed that Pt is reduced at 200 °C. The final material was denoted as CNT/Pt-TiO_2.

Sample preparation

The samples based on CH doped with NPs (CNT-TiO_2) and (CNTPt/TiO_2) were prepared by the solvent casting method using acetic acid (CH_3COOH) as solvent.

The samples were denoted as CH-xCNT-$TiO_{2\text{-}y}$-Gly, where Gly represents glycerol, x is the percentage of CNT in the CNT-TiO_2 composite, and y refers to the mass in g of NPs used (CNT-TiO_2) (mass of CNT-TiO_2 is presented as supporting information, Table S1). The samples were prepared according to the scheme presented in Fig. 1. Briefly, the appropriate amount of NPs was dispersed in 10 mL of 1% CH_3COOH (Sigma Aldrich) and put under ultrasound for 15 min to guarantee uniform distribution of the NPs in the solution, then mixed with 0.20 g of CH (Sigma-Aldrich, MMW, with a degree of deacetylation 75%). The solution was left overnight under magnetic stirring to allow the complete dissolution of the polymer. Then, 0.2 g of Gly (Himedia, 99.5%) was added and the resulting mixture was stirred for 30 min. When the solution became homogeneous, it was poured into a plastic Petri dish. The resulting film was subjected to drying for about two days at room temperature. After this process, the thickness and the mass of the samples were measured using a micrometer (data are presented as supporting information, Table S1).

Characterization techniques

DSC analyses were carried out using a Mettler DSC 821e equipment under a flowing argon atmosphere between – 60 and 300 °C, at a heating rate of 5 °C min^{-1}.

TGA was performed using an STA 490 PC/4/H Luxx Netzsch thermal instrument, between 50 and 900 °C, at a heating rate of 10 ºC min^{-1} and under a nitrogen flow atmosphere.

The total ionic conductivity of the chitosan-based electrolytes was determined using a constant volume support equipped with two gold blocking electrodes located within a Büchi TO 50 oven, and the temperature was measured

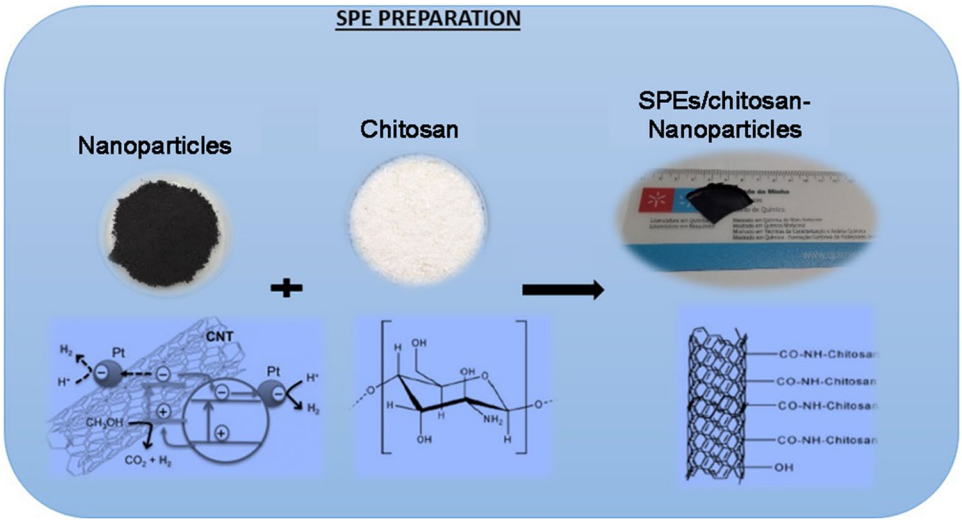

Fig. 1 Scheme for the SPE preparation process

with a K-Type thermocouple localized close to the electrolyte. The impedance measurements were made using an Autolab PGSTAT-12 equipment in a frequency range between 65 kHz and 500 mHz, during heating cycles, and over the temperature range of 19 to about 100 °C, and at approximately 7 ºC intervals.

The electrochemical stability window was evaluated using a two-electrode cell configuration: a 25 µm diameter gold microelectrode as a working electrode and a lithium disk (Aldrich, 99.9%; 19 mm diameter, 0.75 mm thick) as a counter and reference electrode. The cyclic voltammetry (CV) measurements were carried out under an argon atmosphere, at room temperature, within a Faraday cage and recorded by an Autolab PGSTAT-12 (Eco Chemie) at a scan rate of 100 mV s^{-1}.

The polarized optical microscopy (POM) images were recorded using an OPTIKA B-600POL microscope equipped with an 8 M pixel Digital Photo Camera. The images were analyzed using the OPTIKAVision Pro software.

The wettability of the samples was assessed by means of static contact angle measurements using the sessile drop method. Contact angles were measured in a temperature-controlled chamber at 25 ± 1 ºC using a Krüss DSA25S drop shape analyzer controlled by the software ADVANCE. The volume of the liquid droplets was kept constant at 5 µL. Contact angles were measured from digital images acquired by a video camera using the Young–Laplace fitting. The contact angle values were measured at 4 or 5 different spots. At each spot, 5 measurements were performed. The reported results correspond to the average value of all the measurements. The error analysis of the data was implemented by the arithmetic mean of the root mean square error.

Results and discussion

Ionic conductivity

The choice of CNT was based on the electrical performance evaluated in previous work [13]. In this work, the CNT content in the samples was below the percolation threshold to ensure that membranes are electrically insulating. The electronic conductivity of CH-20CNT-$TiO_{2\text{-}0.05}$ was 6.6×10^{-11} S cm^{-1} at 30 ºC and 5.1×10^{-10} S cm^{-1} at 30 °C for CH-20CNT-Pt/$TiO_{2\text{-}0.05}$.

The complex impedance technique is useful for the characterization of ionic conduction processes and analysis of the conductivity behaviour of materials. Typical plots of imaginary impedance (– Z'') versus real impedance (Z') for the electrolytes with CH-1CNT-TiO_{2}-$_{0.05}$ at different temperatures and electrolytes with different CNT-TiO_2 amounts at the same temperature (~ 50 ºC) are shown in Fig. 2a and b, respectively.

Typically, the Nyquist plots show three characteristics parts: a semi-circle located in the high-frequency range which corresponds to the charge transfer process (bulk material properties) [51], a straight line at a lower frequency which is related to the diffusion process, i.e. the sample/electrode interface and the transition between these phenomena [52, 53]. The impedance spectroscopy was analyzed by the equivalent electrical circuit similar to that used to describe gold electrode processes [54, 55]. This equivalent circuit was fitted to the impedance results of samples and showed a good agreement between the experimental results and the equivalent circuit.

The Nyquist plot of Fig. 2a shows a typical semi-circle. Generally, the radius of the semi-circles presented in

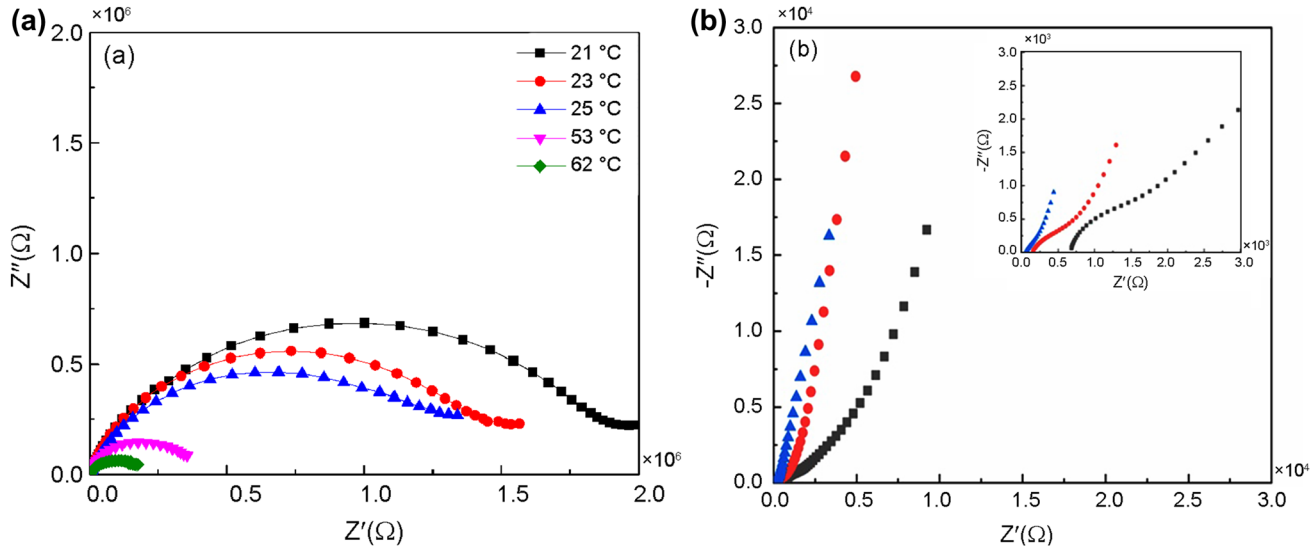

Fig. 2 **a** Nyquist plots for the CH-1CNT-$TiO_{2\text{-}0.05}$ membrane at given temperatures, and **b** Nyquist plots for CH-20CNT-$TiO_{2\text{-}y}$ at 50 ºC (■) y = 0.05; (●) y = 0.10; (▲) y = 0.15

Fig. 2a decreases at increasing temperature. This decrease in the resistive part (ionic resistance calculated in the Z' axis) is due to the decreased bulk resistance, i.e., increase in the charge mobility. The complex impedance curve does not touch the real axis though it is close to it. In these cases, the complex impedance plot is extrapolated to its intersection with the real axis and the conductivity of the membrane is calculated using Osman's method [56].

The linear region is not observed in low-frequency zone, which is probably due to the charge transfer process which is most significant for theCH-1CNT-$TiO_{2\text{-}0.05}$ sample. It must be noted that in the inset of Fig. 2b the semi-circle is practically not observed due to the higher amount of CNTs in these samples. These Nyquist plots demonstrate that the inclusion of CNT attenuates the semi-circle corresponding to the charge transfer process. This result indicates that the presence of the fillers facilitates the charge transfer process due to the increase in electrical conductivity [57].

The intercept of the semi-circle with the real axis gives the bulk resistance (R_b) of the material.

The R_b values were converted into the ionic conductivity (σ) of the electrolytes according to Eq. 1:

$$\sigma = \frac{d}{A \times R_b} \tag{1}$$

where, d is the thickness of the film and A is the contact area between the electrolyte and the electrode. The experimental values of R_b are dependent on the composition of the polymer electrolytes and the temperature as shown in Fig. 2a andb and Table 1.

Table 1 Temperature dependence of the bulk resistance of CH-20CNT-$TiO_{2\text{-}0.05}$ and CH-1CNT-$TiO_{2\text{-}0.05}$

CH-20CNT-$TiO_{2\text{-}0.05}$		CH-1CNT-$TiO_{2\text{-}0.05}$	
T (°C)	Rb (Ω)	T (°C)	Rb (Ω)
21	11.88	32	2196.00
34	9056.20	34	1871.90
50	1683.00	49	1001.70
76	397.39	63	899.05
96	215.35	80	442.58

The transport property in composite materials is a complex process, which is not well understood. It depends on several factors, such as dielectric constant of the host polymer and the mobility of polymer chains. It is of interest to examine the case of CH. This polymer can act as a cationic polyelectrolyte because of its free amino groups [58]. With respect to its ionic properties, the CH membrane has been used for chloride-ions-conducting [59].

From the imaginary and real part plotting of the impedance of CH-1CNT-$TiO_{2\text{-}0.05}$ membranes, it is clear that the incorporation of the CNT-TiO_2NPs induces changes in the conductivity characteristics of the membrane. Particularly at the highest temperatures, the low-frequency semi-circles of CH-1CNT-$TiO_{2\text{-}0.05}$ membranes are much smaller, indicating an improvement of the conductivity and mobility process after hybridization with the CNT-TiO_2 composite. On the other hand, Fig. 2a shows a semi-circle which may be due to the CNT-TiO_2 interface [60].

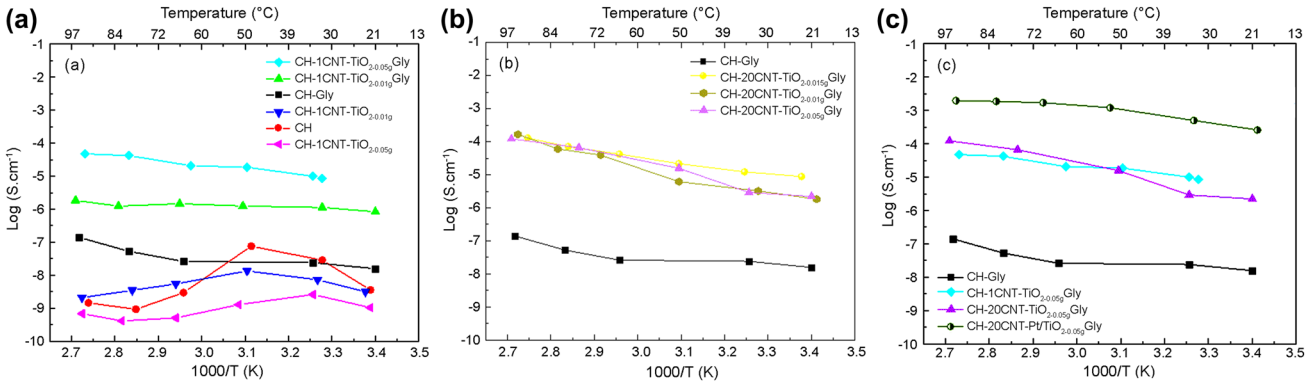

Fig. 3 **a** Ionic conductivity as a function of the temperature of CH-1CNT-TiO_{2-y} for y = 0.05, and 0.01 g with and without Gly, **b** CH-20CNT-TiO_2 y for y = 0.05, 0.10, and 0.15 g with/without Gly, and **c** a comparison between CH Gly, CH-1CNT-$TiO_{2\text{-}0.05}$-Gly, CH-20CNT-$TiO_{2\text{-}0.05}$-Gly and CH- 20CNT-Pt/$TiO_{2\text{-}0.05}$-Gly. All the conductivity values with an experimental error of ± 5%

The ionic conductivity in the temperature range from 25 to 90 °C of samples prepared with CH as a natural matrix and CNT-TiO_2NPs as dopants are presented in Fig. 3a–c.

It should be noticed that Gly has a significant effect on the conductivity of electrolytes, promoting an increase from 1.4×10^{-9} to 1.4×10^{-7} S cm^{-1} at 90 °C for the CH matrix. The marked increase of the ionic conductivity confirms the successful addition of Gly. A small quantity of CH_3COOH may remain in the final materials, but due to its volatility it must have evaporated during the drying process. The residual minor amount of water present in the as-prepared samples is unknown. The amount of Gly would be expected to remain during the synthesis process. However, in these samples, Gly can coexist with the residual water.

As already shown else where Gly acts as a plasticizer and helps promote better conductivity values [61]. The co-existence of Gly in the electrolyte media was beneficial, since this compound, not only plasticized the materials but also increased the concentration of available –OH groups which could also be involved in proton transport.

For electrolytes lacking Gly, the behaviour is quite different. The CH-1CNT-$TiO_{2\text{-}0.05}$ electrolyte has a lower conductivity than the CH matrix, but for the CH-1CNT-$TiO_{2\text{-}0.01}$ electrolyte it is slightly higher, although the latter sample contains less CNT-TiO_2 material. This behaviour may be due to the fact that the CH matrix has some impurities and as it does not have a plasticizing agent, higher amounts of CNT-TiO_2 and other impurities can form some clusters and the consequence is a decrease in the conductivity[62]. On the other hand, for systems with Gly, the addition of CNT-TiO_2NPs clearly increased their conductivity.

Indeed, at 90 °C, the conducivity of CH-1CNT-$TiO_{2\text{-}0.05}$ sample increased from 1.4×10^{-7} to 4.7×10^{-5} S cm^{-1}. As the temperature increased, the ionic conductivity increased as well. This increase may be due to the formation of free volume and unoccupied spaces for the migration of ions.

For the CH-20CNT-$TiO_{2\text{-}0.05}$ sample (Fig. 3b), the addition of NPs improved the conductivity of the electrolytes from 1.4×10^{-7} to 1.22×10^{-4} S cm^{-1} at 90 °C.

The highest conductivity was achieved for a mass of 0.05 g of 20 CNT-TiO_2 (relative to 0.2 g of CH). When a mass of 0.10 g or more of 20 CNT-TiO_2 was added, the conductivity decreased, probably due to the agglomeration of the NPs. The conductivity values for the samples with 0.05, 0.10 and 0.15 g of 20 CNT-TiO_2 are very close, and probably within the experimental error (± 5%). This finding strongly suggests that the competition between the association and dissociation of NPs may occur with almost equal probability, leading to slight changes in conductivity.

Residual water remains inside the polymer. According to Abdulkareem [63], the water molecules absorbed into the CH chains can form hydrogen bonds, thus promoting proton transfer from amino groups to water molecules, accordingly giving rise to proton conductivity. In this work, the proton conductivity of CH films has been interpreted using Grotthuss "structural diffusion" mechanisms. In the Grotthuss mechanism, protons originating from the protonated amino groups can move along the hydrated molecule through hydrogen-bond network hopping process through the breaking/formation of hydrogen bonds, which are followed by a local molecular rearrangement, most often a rotation ("structural diffusion"). In CH films, a combination of both Grotthuss and vehicular mechanisms led to proton conductivity [64]. In summary, it was proposed that both Arrhenius (Grotthuss) and VTF (vehicular) mechanisms govern ionic conductivity in our samples. This approach requires further studies and clearly justifies which one is predominant and correlates with structure, constituents, and temperature.

The ionic conductivity behaviour could be described by the free volume theory and by the Vogel-Tammann-Fulcher (VTF) equation (Eq. 2).

$$\sigma(T) = \sigma_0 e^{\frac{-B}{(T-T_0)}} \quad (2)$$

where σ_0 is constant, B is the pseudo energy of activation, and T_0 is the temperature at which the configurational entropy of the polymer becomes zero and is close to the T_g.

Graphically, the ionic conductivity behaviour is described by the VTF equation when a curved correlation between log σ and 1/T is observed. However, in several polymeric systems the preferred path for ionic movement is a jump from one to another site of complexation (so-called Grotthuss mechanism). This model of ionic conductivity as a function of temperature is described by the Arrhenius equation (Eq. 3).

$$\sigma(T) = \sigma_0 e^{\frac{-E_a}{RT}} \quad (3)$$

where σ_0 is constant, E_a is the energy of activation, R is the gas constant (8.314 J mol^{-1} K^{-1}) and T is the temperature in Kelvin. Therefore, the energy of activation of the sample can be simply obtained from the slope of log σ versus 1/T when this plot is linear.

The experimental points of samples (CH-1CNT-TiO_2-0.05Gly, CH-20CNT-TiO_2-0.05Gly and CH-20CNT-Pt/TiO_2-0.05Gly) were fitted with a straight line and all regression values are close to unity, suggesting that the variations of conductivity with temperature can be elucidated with Arrhenius rule.

E_a was calculated from the slopes of the logσ versus 1000/T graphs, and values extracted from fittings. These values are 98.94 J.mol^{-1} for the more conductive sample (CH-20CNT-Pt/TiO_2-0.05Gly) and 208.68 and 311.77 J.mol^{-1} for samples CH-1CNT-TiO_2-0.05Gly and CH-20CNT-TiO_2-0.05Gly, respectively. Figure 3c presents a comparison of the conductivity curves between samples produced with the same amount of 1CNT-TiO_2, 20CNT-TiO_2, and 20CNT-Pt/TiO_2 composites (0.05 g). This graph reveals that the conductivities of the samples with 20CNT-TiO_2 and 1CNT-TiO_2 are very similar. Probably the increase of the CNT content facilitates the aggregation of the NPs and consequently the decrease of proton exchange.

When Pt was added to 20CNT- TiO_2, the conductivity increased. Undoubtedly, the presence of Pt on the surface of 20CNT-$TiO_{2\text{-}0.05}$ promoted the catalyst activity, thus contributing to the improvement of the ionic conductivity. The ionic conductivity values increased from 1.2×10^{-4} to 1.9 10^{-3} S cm^{-1} at 90 °C. Consequently, Pt could serve as a support to the interactions of the interface in the CNT and TiO_2. Besides, it may improve the association between the NPs and CH and also improve the charge transfer in the interface. Normally, noble metals, such as Pt, induce enhanced change transfer. Platinum improves the catalyst properties [65, 66] and gives high specific activity for activity per surface area of the catalyst surface and in its practical applications. The amount of Pt used enhances the activity of electrocatalysts. In addition, carbon materials (CNTs) have high surface areas and suitable porosity, allowing for high dispersion of Pt and accelerated charge transfer in the electrolyte [67]. The combination of Pt-based catalysts with metal oxide materials as catalyst supports (e.g., Pt/TiO_2, Pt/CeO_2, Pt/WO_3) has been actively studied to discover the potential advantages of these combined materials for applications in direct methanol fuel cells [68]. We believe that the reports here open new opportunities for fundamental research and applications.

Cyclic voltammetry

Cyclic voltammogram of the CH-20CNT-$TiO_{2\text{-}0.05}$ was registered over the potential range from -2.0 to 6.0 V at room temperature and at a scan rate of 100 mV s^{-1} (results not shown). The voltammogram shows that the sample is stable in the anodic region up to about 3.0 V versus Li/Li^+, whereas in the cathodic region, it is stable as high as -1.0 V versus Li/Li^+. This means that the overall redox stability of the sample spans about 4.0 V, an indication that these materials display an acceptable stability window for an application in solid-state devices.

Thermal behaviour

The thermal behaviour of materials is a very important condition that must be fulfilled to envisage possible practical applications. Thermal analysis provides important insights into the degree of crystallinity, melting point (T_m) and glass transition temperature (T_g) [69].

The DSC curves of CH electrolytes doped with different amounts of CNT- TiO_2 composites and containing Gly are shown in Figs. 4a–c. At around 100–170 ºC, the CH matrix sample shows a noticeable endothermic peak (T_m) that probably corresponds to the loss of absorbed water overlapped with its fusion. When CH/CNT-TiO_2 samples are subjected to a temperature increase, absorbed water is released `at different temperatures from 90 to 170 ºC (peak position shifted), due to the different interactions of water with CH, CNT and TiO_2. On the other hand, the T_g of CH is not detected. T_g of CH is usually estimated at about 203 ºC [70], but it is known that the addition of plasticizers such as Glycan leads to its decrease.

The onset of thermal decomposition was observed above 260 ºC. The presence of CNTs was expected to interfere with the chain motion of the CH matrix. A difference between the T_{onset} of 1CNT-TiO_2, 20CNT-TiO_2, 20CNT-Pt/TiO_2 and

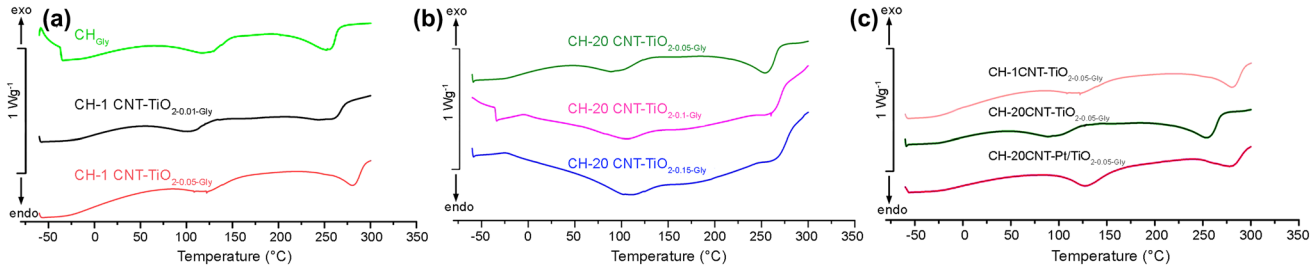

Fig. 4 **a** DSC thermograms of CH-Gly, CH-1CNT-TiO_{2-y}Gly for y = 0.05 and 0.01 g, **b** DSC thermograms of CH-20CNT-TiO_{2-y}Gly for y = 0.05, 0.1, and 0.15 g, and **c** comparison of DSC thermograms of CH-1CNT-TiO_{2}-$_{0.05}$-Gly, CH-20CNT-TiO_{2}-$_{0.05}$-Gly and CH- 20CNT-Pt/TiO_{2}-$_{0.05}$-Gly

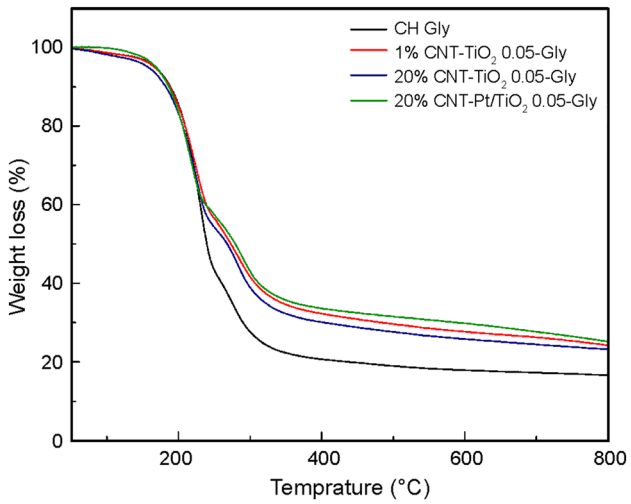

Fig. 5 TGA thermograms of selected samples

the CH matrix (250 °C) was observed, suggesting a stabilizing effect provided by the introduction of the CNT-TiO_2 materials.

The samples thermal stability was thoroughly evaluated by TGA. Fig. 5 displays the TGA thermograms obtained for the same samples included in this study and these results do not show a stabilizing effect upon introduction of the CNT-TiO_2 materials, as suggested by DSC (doped samples start their degradation at a higher temperature). All materials show two-stage degradation process probably due to the different interactions of Gly and the nanoparticles with the polysaccharide chain [71]. The first degradation starts at about 130–150 ºC, and the second step is about 240–300 ºC. In the case of the present study, beyond about 400 ºC the degradation process ends and the weight loss continues slowly as the temperature increases toward the maximum analyzed temperature of 800 ºC.

The decomposition temperatures obtained are considered acceptable for most of the envisaged practical applications.

Polarized optical microscopy (POM)

The POM images of selected samples (CH; CH-Gly) are shown in Fig. 6. These results prove that the electrolytes are birefringent. The anisotropy of these samples suggests that crystalline phases are formed at the submicrometer scale.

Wettability

The static water contact angle measured for CH was 100.73 ± 12.93 ° (Fig. 7 and Table 2), revealing the hydrophobic behavior of the CH matrix. After inclusion of Gly, the value of the contact angle decreased to 88.53 ± 3.63°, indicating an increase in the hydrophilicity of the CH-Gly film. The contact angle values obtained for membranes

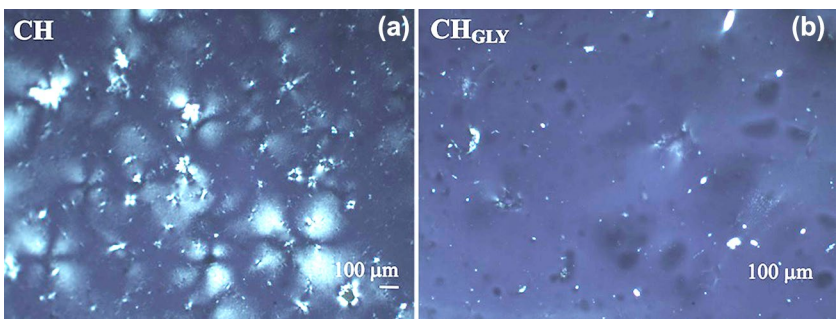

Fig. 6 POM images of SPEs: CH; CH-Gly

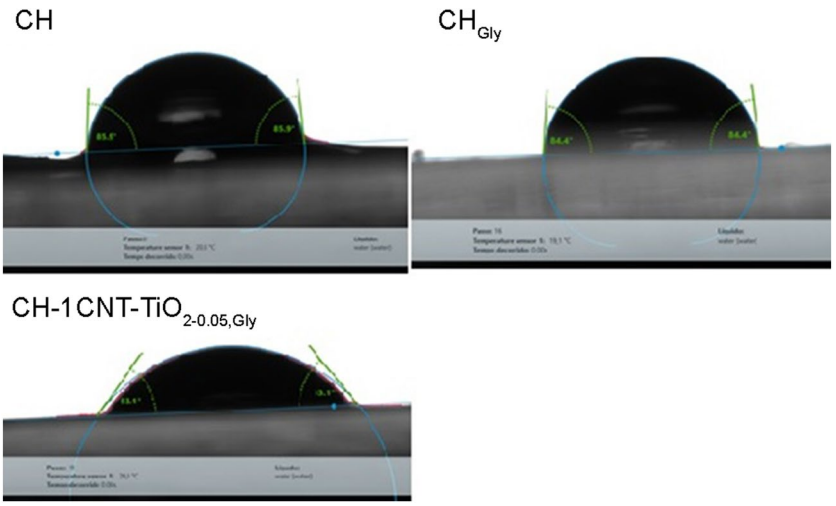

Fig. 7 Selected micrographs of static water contact angle measurements of SPEs: CH; CH-Gly and CH-1CNT-$TiO_{2\text{-}0.05}$-Gly samples

Table 2 Contact angles at the air–liquid (ultrapure water)-solid (CH-xCNT-TiO_2-y films) surface

Sample	Sessile drop contact angle (θ°), medium value (°, degrees)
CH film	100.73 (±12.93) °
CH-1CNT-TiO_2-0.01	91.82 (±2.24) °
CH-1CNT- TiO_2-0.05	83.66 (±3.63) °
CH-Glyfilm	88.53 (±3.38) °
CH-1CNT-$TiO_{2\text{-}0.01,}$ Gly	90.02 (±3.63) °
CH-1CNT-$TiO_{2\text{-}0.05,}$ Gly	74.10 (±6.51) °
CH-20CNT-$TiO_{2\text{-}0.05,}$ Gly	54.53 (±6.63) °
CH-20CNT-$TiO_{2\text{-}0.10,}$ Gly	71.03 (±15.50) °
CH-20CNT-$TiO_{2\text{-}0.15,}$ Gly	76.92 (±4.19) °
CH-20CNT-Pt/$TiO_{2\text{-}0.05,}$ Gly	60.49 (±5.54) °

progressively decreased upon further inclusion of the CNT-TiO_2 hybrids, leading to the enhancement of the hydrophilicity of the materials. This result was somewhat expected, given the marked hygroscopic character of both the CNT and TiO_2 phases.

Conclusion

New composites were prepared through solvent casting method using CH complexed with CNT/TiO_2 and containing Gly. The purpose of using CNT/TiO_2 nanocomposites was to improve the intrinsic properties (conductivity and mechanical) of the matrix considered. The presence of CNT significantly decreases the energy required for the conductive process and increases the free volume of the polymer, leading to higher ion mobility.

The highest ionic conductivity value of 1.96×10^{-3} S cm^{-1} at 90 ºC were obtained for the 20CNT-Pt/TiO_2sample. The significant effect of Gly on the conductivity of the electrolytes is noteworthy. In addition, the presence of Pt improved clearly the charge transfer in the membrane electrolyte, hence leading to the increase in the conductivity. Furthermore, the conductivity measurements in the obtained composites allowed some evidence of CNT-TiO_2 influence in the transfer of current through the CH matrix.

The electrochemical stability evaluated by cyclic voltammetry revealed a stable window operation up to 4.0 V. These results imply that incorporating CNT into the CH matrix may provide a novel way to fabricate proton membranes for fuel cell applications.

Supplementary Information The online version contains supplementary material available at https://doi.org/10.1007/s13726-022-01069-1.

Acknowledgements The authors are grateful for the Fundação para a Ciência e Tecnologia (FCT) through the Chemistry Research Centre of the University of Minho (UID/QUI/00686/2019 and UID/QUI/0686/2020), CQ-VR of the UTAD (UID/QUI/00686/2013), LUMECD (POCI-01-0145-FEDER-016884 and PTDC/CTM-NAN/0956/2014). Also this work was financially supported by: LA/P/0045/2020 (ALiCE), UIDB/50020/2020 and UIDP/50020/2020 (LSRE-LCM) funded by national funds through FCT/MCTES (PIDDAC); project POCI-01-0145-FEDER-006984. M. Fernandes acknowledges FCT-UTAD for the contract in the scope of Decreto-Lei 57/2016-Lei 57/2017.

References

1. Hu C, Xiao Y, Zou Y, Dai L (2018) Carbon-based metal-free electrocatalysis for energy conversion, energy storage, and environmental protection. Electrochem Energy 1:238–238
2. Nasirinezhad M, Ghaffarian SR, Tohidian M (2021) Eco-friendly polyelectrolyte nanocomposite membranes based on chitosan and

sulfonated chitin nanowhiskers for fuel cell applications. Iran Polym J 30(4):355–367
3. Shen H, Yi E, Cheng L, Amores M, Chen G, Sofie SW, Doeff MM (2019) Solid-state electrolyte considerations for electric vehicle batteries. Sustain Energy Fuels 3(7):1647–1659
4. Zheng F, Kotobuki M, Song S, Lai MO, Lu L (2018) Review on solid electrolytes for all-solid-state lithium-ion batteries. J Power Sources 389:198–213
5. Li J, Ma C, Chi M, Liang C, Dudney NJ (2015) Solid electrolyte: the key for high-voltage lithium batteries. Adv Energy Mater 5:1401408
6. Alaswad A, Omran A, Sodre JR, Wilberforce T, Pignatelli G, Dassisti M, Baroutaji A, Olabi AG (2021) Technical and commercial challenges of proton-exchange membrane (Pem) fuel cells. Energies 14(1):144
7. Chandan A, Hattenberger M, El-Kharouf A, Du S, Dhir A, Self V, Pollet BG, Ingram A, Bujalski W (2013) High temperature (HT) polymer electrolyte membrane fuel cells (PEMFC). J Power Sources 231:264–278
8. Wright PV (1975) Electrical conductivity in ionic complexes of poly(ethylene oxide). Br Polym J 7:319–327
9. Armand M (1994) The history of polymer electrolytes. Solid State Ionics 69:309–319
10. Ahmed S, Cai Y, Ali M, Khanal S, Xu S (2019) Preparation and performance of nanoparticle-reinforced chitosan proton-exchange membranes for fuel-cell applications. J Appl Polym Sci 136:46904
11. Aziz SB, Abidin ZH (2013) Electrical conduction mechanism in solid polymer electrolytes: new concepts to arrhenius equation. J Soft Matter. https://doi.org/10.1155/2013/323868
12. Millet P, Dragoe D, Grigoriev S, Fateev V, Etievant CA (2009) research program on PEM water electrolysis supported by the European Commission. Int J Hydrog Energy 34:4974–4982
13. Zhao S, Yang Y, Zhong F, Niu W, Liu Y, Zheng G, Liu H, Wang J, Xiao Z (2021) Fabrication of composite polymer electrolyte membrane using acidic metal-organic frameworks-functionalized halloysite nanotubes modified chitosan. Polymer 226:123800
14. Andrade JR, Raphael E, Pawlicka A (2009) Plasticized pectin-based gel electrolytes. Electrochim Acta 54:6479–6483
15. Alves RD, Rodrigues LC, Andrade JR, Fernandes M, Pinto JV, Pereira L, Pawlicka A, Martins R, Fortunato E, deZeaBermudez V, Silva MM (2013) Gelatinn $Zn(CF_3SO_3)_2$ polymer electrolytes for electrochromic devices. Electroanalysis 25:1483–1490
16. Nik Aziz NA, Idris NK, Isa MI (2010) Solid polymer electrolytes based on methylcellulose: FT-IR and ionic conductivity studies. Int J Polym Anal Charact 15:319–327
17. Hanna Rosli NA, Loh KS, Wong WY, Yunus RM, Lee TK, Ahmad A, Chong ST (2020) Review of chitosan-based polymers as proton exchange membranes and roles of chitosan-supported ionic liquids. Int J Mol Sci 21(2):632
18. Sarode S, Upadhyay P, Khosa MA, Mak T, Shakir A, Song S, Ullah A (2019) Overview of wastewater treatment methods with special focus on biopolymer chitin-chitosan. Int J Biol Macromol 121:1086–1100
19. Alves R, Sentanin F, Sabadini RC, Pawlicka A, Silva MM (2018) Green polymer electrolytes of chitosan doped with erbium triflate. J Non Cryst Solids 482:183–191
20. Wang X, Zhou P, Lv X, Liang Y (2021) Insight into the structure-function relationships of the solubility of chitin/ chitosan in natural deep eutectic solvents. Mater Today Commun 27:102374
21. Gbenebor OP, Adeosun SO, Lawal GI, Jun S, Olaleye SA (2017) Acetylation, crystalline and morphological properties of structural polysaccharide from shrimp exoskeleton. Eng Sci Technol 20:1155–1165
22. Nakayama RI, Katsumata K, Niwa Y, Namiki N (2020) Dependence of water-permeable chitosan membranes on chitosan molecular weight and alkali treatment. Membranes 10:351
23. Aziz SB, Asnawi AS, Mohammed PA, Abdulwahid RT, Yusof YM, Abdullah RM, Kadir MF (2021) Impedance, circuit simulation, transport properties and energy storage behavior of plasticized lithium ion conducting chitosan based polymer electrolytes. Polym Test 101:107286
24. De Oliveira ACS, Ugucioni JC, Borges SV (2021) Effect of glutaraldehyde/glycerol ratios on the properties of chitosan films. J Food Process Preserv 45:15060
25. Hadi JM, Aziz SB, Kadir MF, El-Badry YA, Ahamad T, Hussein EE, Asnawi AS, Abdullah RM, Alshehri SM (2021) Design of plasticized proton conducting chitosan: dextran based biopolymer blend electrolytes for EDLC application: structural, impedance and electrochemical studies. Arab J Chem 14:103394
26. Galicia-Aguilar JA, López-Badillo M, García-Castro MA, Varela-Caselis JL, Solís-Martínez C, Ortega-Pérez J (2021) Effect of the concentration of glycerin in the performance of chitosan membranes utilised in aqueous phase permeation. Rev Mex Ing Quim 20:87–96
27. Schaffer JV, Lupatini KN, Machado B, Silva ES, Ferracin RJ, Alves HJ (2018) Parameters effect on proton conductivity to obtain chitosan membranes for use as electrolytes in PEMFC. Int J Energy 42:1381–1385
28. Murata K, Izuchi S, Yoshihisa Y (2000) An overview of the research and development of solid polymer electrolyte batteries. Electrochim Acta 45:1501–1508
29. Karmakar A, Ghosh A (2011) Charge carrier dynamics and relaxation in (polyethylene oxide-lithium-salt)-based polymer electrolyte containing 1-butyl-1-methylpyrrolidinium bis (trifluoromethylsulfonyl)-imide as ionic liquid. Phys Rev E 84:051802
30. DasS GA (2015) Ion conduction and relaxation in PEO-LiTFSI-Al_2O_3 polymer nanocomposite electrolytes. J Appl Phys 117:17
31. Pal P, Ghosh A (2018) Influence of TiO_2 nano-particles on charge carrier transport and cell performance of PMMA-$LiClO_4$based nano-composite electrolytes. Electrochim Acta 260:157–167
32. Ahmed S, Arshad T, Zada A, Afzal A, Khan M, Hussain A, Hassan M, Ali M, Xu S (2021) Preparation and characterization of a novel sulfonated titanium oxide incorporated chitosan nanocomposite membranes for fuel cell application. Membranes 11:450
33. Wang J, Gong C, Wen S, Liu H, Qin C, Xiong C, Dong L (2019) A facile approach of fabricating proton exchange membranes by incorporating polydopamine functionalized carbon nanotubes into chitosan. Int J Hydrog Energy 44:6909–6918
34. Mallakpour S, Azadi E, Hussain CM (2021) Chitosan/carbon nanotube hybrids: recent progress and achievements for industrial applications. New J Chem 45:3756–3777
35. Ahn CH, Baek Y, Lee C, Kim SO, Kim S, Lee S, Kim SH, See S, Bae SS, Park J, Yoon J (2012) Carbon nanotube-based membranes: fabrication and application to desalination. J Ind Eng Chem 18(5):1551–1559
36. de Lannoy CF, Jassby D, Davis DD, Wiesner MR (2012) A highly electrically conductive polymer–multiwalled carbon nanotube nanocomposite membrane. J Membr Sci 415:718–724
37. Thirugnanam L, Palanisamy M, Kaveri S, Ramaprabhu S, Pol VG, Dutta M (2021) TiO_2 nanoparticle embedded nitrogen doped electrospun helical carbon nanofiber-carbon nanotube hybrid anode for lithium-ion batteries. Int J Hydrog Energy 46(2):2464–2478
38. Wang ZY, Lu ZX, Guo W, Luo X, Yin YH, Liu XB, Li YS, Xia BY, Wu ZP (2021) A dendrite-free lithium/carbon nanotube hybrid for lithium-metal batteries. Adv Mater 33:2006702

39. Narsimulu D, Kakarla AK, Yu JS (2021) Cerium vanadate/carbon nanotube hybrid composite nanostructures as a high-performance anode material for lithium-ion batteries. J Energy Chem 58:25–32
40. Ahn JH, Kim YJ, Wang GX (2006) Electrochemical properties of carbon nanotube-dispersed PEO-LiX electrolytes. Met Mater Int 12:69–73
41. Nunes-Pereira J, Lopes AC, Costa CM, Leones R, Silva MM, Lanceros-Méndez S (2012) Porous membranes of montmorillonite/poly (vinylidene fluoride-trifluorethylene) for Li-ion battery separators. Electroanalysis 24(11):2147–2156
42. Nunes-Pereira J, Lopes AC, Costa CM, Rodrigues LC, Silva MM, Lanceros-Méndez S (2013) Microporous membranes of NaY zeolite/poly (vinylidene fluoride–trifluoroethylene) for Li-ion battery separators. J Electroanal Chem 689:223–232
43. Hasegawa K, Gunji H, Kijima R, Eguchi M, Nishitani-Gamo M, Ando T, Nakagawa K (2021) Electrochemical performance of marimocarbon/lithium titanate composites synthesized by hydrothermal method for lithium-ion batteries. J Mater Sci 56:16602–16611
44. Sang Sim G, Santhoshkumar P, Park JW, Ho CW, Shaji N, Kim HK, Nanthagopal M, Lee CW (2021) Chitosan-derived nitrogen-doped carbon on $Li_2ZnTi_3O_8/TiO_2$ composite as an anode material for lithium-ion batteries. Ceram Int 47(23):33554–33562
45. Wang J, Gong C, Wen S, Liu H, Qin C, Xiong C, Dong L (2018) Proton exchange membrane based on chitosan and solvent-free carbon nanotube fluids for fuel cells applications. Carbohydr Polym 186:200–207
46. Ikram R, Mohamed Jan B, Abdul Qadir M, Sidek A, Stylianakis MM, Kenanakis G (2021) Recent advances in chitin and chitosan/graphene-based bio-nanocomposites for energetic applications. Polymers 13(19):3266
47. Xia Y, He Y, Zhang F, Liu Y, Leng J (2021) A review of shape memory polymers and composites: mechanisms, materials, and applications. Adv Mater 33(6):2000713
48. Nasirinezhad M, Ghaffarian SR, Tohidian M (2021) Eco-friendly polyelectrolyte nanocomposite membranes based on chitosan and sulfonated chitin nanowhiskers for fuel cell applications. Iran Polym J 30(4):355–367
49. Wang W, Shan B, Zhu L, Xie C, Liu C, Cui F (2018) Anatase titania coated CNTs and sodium lignin sulfonate doped chitosan proton exchange membrane for DMFC application. Carbohydr Polym 187:35–42
50. Naffati N, Sampaio MJ, Da Silva ES, Nsib MF, Arfaoui Y, Houas A, Faria JL, Silva CG (2020) Carbon-nanotube/TiO_2 materials synthesized by a one-pot oxidation/ hydrothermal route for the photocatalytic production of hydrogen from biomass derivatives. Mater Sci Semicond Process 115:105098
51. Rahman NA, Hanifah SA, Mobarak NN, Ahmad A, Ludin NA, Bella F, Su'ait MS (2021) Chitosan as a paradigm for biopolymer electrolytes in solid-state dye-sensitised solar cells. Polymer 230:124092
52. Chang BY, Park SM (2010) Electrochemical impedance spectroscopy. Annu Rev Anal Chem 3(1):207–229
53. Xiao L, Zhen Q, Hao F, Ted L, Ran P, Zhijie L, James MR, Xinyu L (2021) Enhancing the performance of paper-based electrochemical impedance spectroscopy nanobiosensors: an experimental approach. Biosens Bioelectron 177:112672
54. Bondarenko AS (2005) Potentiodynamic electrochemical impedance spectroscopy of lead upd on polycrystalline gold and on selenium atomic underlayer. Electrochem Commun 7(6):631–636
55. Kerner Z, Pajkossy T (2002) Measurement of adsorption rates of anions on Au (111) electrodes by impedance spectroscopy. Electrochim Acta 47:2055–2063
56. Osman Z, Ibrahim ZA, Arof AK (2001) Conductivity enhancement due to ion dissociation in plasticized chitosan based polymer electrolytes. Carbohydr Polym 44:167–173
57. Karaman ES, Wang Z, Chen K, Siddiqui Z, Cheng Y, Basuray S, Kumar V, Mitra S (2021) Functionalized carbon nanotube doped gel electrolytes with enhanced mechanical and electrical properties for battery applications. Mater Chem Phys 264:124448
58. Carvalho SG, dos Santos AM, Silvestre ALP, Meneguin AB, Barboza Ferreira LM, Chorilli M, Gremiao MP (2021) New insights into physicochemical aspects involved in the formation of polyelectrolyte complexes based on chitosan and dextran sulfate. Carbohydr Polym 271:118436
59. Compañ V (2021) Polymeric membranes. Membranes 11:294
60. John JP, Nancy TM, Sharmila TB (2021) A comprehensive review on the environmental applications of graphene–carbon nanotube hybrids: recent progress, challenges and prospects. Mater Adv 2:6816–6838
61. Johari SN, Tajuddin NA, Hanibah H, Deraman SK (2021) A review: ionic conductivity of solid polymer electrolyte based polyethylene oxide. Int J Electrochem 16:211049
62. Du JF, Bai Y, Chu WY, Qiao LJ (2010) The structure and electric characters of proton-conducting chitosan membranes with various ammonium salts as complexant. J Polym Sci Part B 48:880–885
63. Abdulkareem SS (2021) Structural, morphological and electrical properties of chitosan/methylcellulose blend polymer doped with different concentrations of NH_4NO_3. Mater Res Express 8:086301
64. Pawlicka A, Mattos RI, Tambelli CE, Silva IDA, Magon CJ, Donoso JP (2013) Magnetic resonance study of chitosan biomembranes with proton conductivity properties. J Membr Sci 429:190–196
65. Prater KB (1994) Polymer electrolyte fuel cells: a review of recent developments. J Power Sources 51(1–2):129e44
66. Wilson MS, GottesfeldS, (1992) High performance catalyzed membranes of ultra-low pt loadings for polymer electrolyte fuel cells. J ElectrochemSoc. 139(2):L28e30
67. Ren X, Lv Q, Liu L, Liu B, Wang Y, Liu A, Wu G (2020) Current progress of Pt and Pt-based electrocatalysts used for fuel cells. Sustain Energy Fuels 4(1):15–30
68. Yanga G, Zhang Q, Yua H, Pengc F (2021) Platinum-based ternary catalysts for the electro-oxidation of ethanol. Particuology 58:169–186
69. Agrawal RC, Pandey GP (2008) Solid polymer electrolytes: materials designing and all-solid-state battery applications: an overview. J Phys D Appl Phys 41:223001
70. Sakurai K, Maegawa T, TakahashiT, (2000) Glass transition temperature of chitosan and miscibility of chitosan/poly(*N*-vinyl pyrrolidone) blends. Polymer 41:7051–7056
71. Ahmadi P, Nazeri N, Derakhshan MA, Ghanbari H (2021) Preparation and characterization of polyurethane/chitosan/CNT nanofibrous scaffold for cardiac tissue engineering. Int J Biol Macromol 180:590–598

Authors and Affiliations

Naima Naffati[1,2,3] · Mariana Fernandes[4] · Verónica de Zea Bermudez[4] · Mohamed Faouzi Nsib[2,5] · Youssef Arfaoui[6] · Ammar Houas[2] · Joaquim Luis Faria[3,7] · Cláudia Gomes Silva[3,7] · Maria Manuela Silva[1]

1 Center of Chemistry, Department of Chemistry, University of Minho, 4710-057 Braga, Portugal

2 Research Laboratory of Catalysis and Materials for Environment and Processes, University of Gabes, City Riadh Zerig, Gabes 6029, Tunisia

3 Laboratory of Separation and Reaction Engineering-Laboratory of Catalysis and Materials (LSRE-LCM), Faculdade de Engenharia, University of Porto, RuaDr. Roberto Frias s/n, 4200-465 Porto, Portugal

4 Department of Chemistry and CQ-VR, University of Trás-os-Montes E Alto Douro, 5000-801 Vila Real, Portugal

5 NANOMISENE, CRMN Sousse, Higher School of Sciences and Technology of Hammam Sousse, Sousse, Tunisia

6 Laboratory of Characterizations, Applications and Modeling of Materials (LR18ES08), Department of Chemistry, University of Tunis El Manar, Tunis, Tunisia

7 Present Address: ALiCE - Associate Laboratory in Chemical Engineering, Faculty of Engineering, University of Porto, Rua Dr. Roberto Frias, 4200-465 Porto, Portugal